EERA DeepWind'2016, 13th Deep Sea Offshore Wind R&D Conference

Correlation between Acceleration and Drivetrain Load Effects for Monopile Offshore Wind Turbines

Amir Rasekhi Nejad[a,b,*], Erin E. Bachynski[a,b,c], Lin Li[a,b], Torgeir Moan[a,b]

[a]*Centre for Ships and Ocean Structures (CeSOS), Norwegian University of Science and Technology (NTNU)*
[b]*Centre for Autonomous Marine Operations and Systems (AMOS), Department of Marine Technology, NTNU*
[c]*The Norwegian Marine Technology Research Institute (MARINTEK), Trondheim, Norway*

Abstract

This paper investigates the correlation between the tower-top axial acceleration and the load effects in drivetrain components in a monopile (bottom-fixed) offshore wind turbine. In designing offshore wind turbines, it is a common practice to set a limit for axial acceleration. The main objective of this work is to evaluate the rationality of this assumption as a design criterion for critical components in the drivetrain such as gears and bearings, and to provide guidance for designing the drivetrains in monopile wind turbines. In this study, a 5-MW offshore wind turbine on a monopile structure is modelled and the load effects in the drivetrain are calculated through a de-coupled analysis approach. For each chosen wind speed, the most probable significant wave height and period was chosen from a site in the North Sea with water depth of 29 m which is similar to Dogger Bank wind farm. The results reveal that the life of components inside the gearbox are not correlated with the maximum axial acceleration for the monopile structure. The load effect or life of the first main bearing in the 4-point support is directly correlated with the wind speed while the second main bearing, which carries the axial loads is uncorrelated. The tower-top bending moment, which is an important parameter in designing the main shaft, is found to be highly correlated with the wind speed, not necessarily with the axial acceleration.

Keywords: wind turbine gears; axial acceleration; drivetrain; monopile

1. Introduction

Offshore wind turbines in Europe have been rapidly developing with a 200% increase in installed turbines in the first half of 2015 compared with the same period in 2014 [1]. Today the International Electrotechnical Commission (IEC) design code 61400-3 [2], "Design Requirements for Offshore Wind Turbines", covers the basic design requirements, while the gearbox design is addressed by the IEC 61400-4 [3]. While it is not explicitly specified in the design codes, there is a common practice in the industry to set a limit for the maximum axial acceleration on the tower-top in the range of 0.2g-0.3g, in particular for the floating wind turbines. There is, however, a question whether this limit is rational.

* Corresponding author. Tel.: +47-735-91546 ; fax: +47-735-95528.
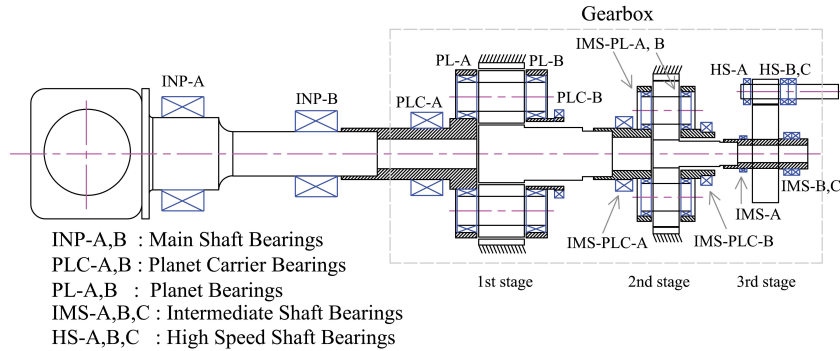 *E-mail address:* Amir.Nejad@ntnu.no.

Fig. 1: Layout of 5 MW reference drivetrain [11].

The structural response of the offshore wind turbines have been evaluated in many earlier studies (e.g. Andersen et al. [4] for monopiles or Bachynski and Moan [5] for a floating turbine). The drivetrain local responses have also been studied (e.g. by Xing et al. [6] and Nejad et al. [7]). However, the influence of the axial tower-top acceleration appears to be not investigated in these earlier studies.

In this study the effect of tower-top maximum axial acceleration on the drivetrain installed on a monopile offshore wind turbine is investigated. Monopile wind turbines are installed in shallow water and are subjected to both wind and wave loads. In this study, the NREL 5-MW reference offshore wind turbine [8] is modelled on a monopile structure. The de-coupled analysis approach is employed. The global analysis is first carried out (using the SIMO-RIFLEX-AeroDyn simulation tools [9]) for chosen environmental conditions with an operational turbine. For each chosen wind speed, the most probable significant wave height and period were chosen from the "North Sea Centre" site from the MARINA platform project [10] with water depth of 29 m. This depth is similar to the Dogger Bank wind farm, which has depths from 15 to 36 m. For each environmental condition, 6 simulations, each 10 min., are carried out.

Second, the forces/moments and motions obtained from the global analysis are applied on a detailed multibody (MBS) drivetrain model, for some of the environmental conditions. The 5-MW reference drivetrain is used [11] and the load effects on gears and bearings are obtained.

2. Wind Turbine & Drivetrain Model

The wind turbine under consideration is the NREL 5 MW reference turbine [8], supported by the monopile foundation from the OC3 study [12]. The water depth in the simulations is taken to be 20 m, consistent with the monopile design. The modelled structure is shown in Fig. 2a in Section 3.2. The pile end is 56 m below the still water level (SWL), while the hub-height is 90 m above SWL. The first fore-aft natural frequency of the complete structure is 4.08 s.

In this study, the 5 MW reference offshore drivetrain [11] was used. This is a 3-stage, 4-point support drivetrain with two main bearings and two torque arms. The two main bearing configuration significantly reduces the non-torque loads which enter the gearbox [7]. Figure 1 shows the layout of the drivetrain. The first main bearing (INP-A) carries the radial load while the axial load is supported by INP-B. The first and second stages are planetary spur gears and the third stage is parallel helical gears.

The general specification of the gearbox is presented in Table 1.

3. Methodology

3.1. Environmental Conditions & Load Cases

The wind and wave data from the "North Sea Centre", site 15 in Li et al. [10] was chosen for the analysis. This site is suitable for monopile foundations with an average water depth of 29 *m*, and the location is close to the Dogger

Table 1: 5-MW Reference Gearbox Specifications [11].

Parameter	Value
Type	2 Planetary + 1 Parallel
1st stage ratio	1:3.947
2nd stage ratio	1:6.167
3rd stage ratio	1:3.958
Total ratio	1:96.354
Rated input shaft speed (rpm)	12.1
Rated input shaft torque (kN.m)	3,946
Total dry mass (×1,000 kg)	53

Bank wind farm. The wave conditions are applied in the 20 m water depth without modification. It should be noted that the long-term wave data for very shallow water is associated with large uncertainties and a simplified model for wave kinematics is employed in the global analysis.

The environmental data was hourly sampled and generated from a hindcast model from 2001 to 2010. Long-term joint distributions of the mean wind speed (U_w), significant wave height (H_s) and spectral peak period (T_p) were obtained by fitting analytical distributions with the hindcast data. The joint distribution of U_w, H_s, and T_p (Eq. 1) consists of a marginal distribution of U_w which follows a two-parameter Weibull distribution, a conditional distribution of H_s given U_w which also follows a two-parameter Weibull distribution, and a conditional distribution of T_p given both U_w and H_s which follows a lognormal distribution.

$$f_{U_w,H_s,T_p}(u,h,t) = f_{U_w}(u) \cdot f_{H_s|U_w}(h|u) \cdot f_{T_p|U_w,H_s}(t|u,h) \tag{1}$$

where $f()$ refers to probability density function (*PDF*). The fitting methods and the parameters for the joint distribution at this site can be found in Li et al. [10].

For the present study, 24 environmental conditions (*ECs*) are selected for the global analysis, while 10 of them, covering the whole range of operational conditions, are further used in the detailed multi-body simulations (*MBS*). The U_w at the hub height (90 m) ranges from the cut-in wind speed (3 m/s) to the cut-out wind speed (25 m/s) with a bin size of 1 m/s. The rated wind speed (11.4 m/s) is also included in the analysis. The most probable mean wind speed for this site is about 9 m/s at hub height.

The corresponding H_s for each U_w is chosen as the most probable value from the conditional distribution of H_s given U_w, i.e., $f_{H_s|U_w}(h|u)$ in Eq. (1), while the T_p values are the most probable values from the conditional distribution of T_p given both U_w and H_s, i.e., $f_{T_p|U_w,H_s}(t|u,h)$ in Eq. (1).

Table 2 lists the selected 24 *ECs*.

Table 2: Environmental conditions.

EC	1	2	3	4	5	6	7	8	9	10	11	12
U_w (m/s)	3	4	5	6	7	8	9	10	11	11.4	12	13
H_s (m)	0.59	0.72	0.85	1	1.17	1.34	1.52	1.72	1.92	2	2.13	2.35
T_p (s)	6.38	6.32	6.28	6.27	6.31	6.35	6.41	6.5	6.59	6.62	6.69	6.81
used in MBS	√		√		√		√			√		√
EC	13	14	15	16	17	18	19	20	21	22	23	24
U_w (m/s)	14	15	16	17	18	19	20	21	22	23	24	25
H_s (m)	2.57	2.81	3.05	3.3	3.55	3.81	4.08	4.35	4.63	4.92	5.21	5.5
T_p (s)	6.92	7.06	7.19	7.33	7.47	7.62	7.78	7.93	8.09	8.27	8.43	8.6
used in MBS				√			√			√		√

3.2. De-coupled Approach

A de-coupled analysis approach was used in this study. The difference in natural frequencies in global and local drivetrain models as well as the computational requirements for complex gearbox models justify using a de-coupled analysis approach [13]. This method has been used in earlier studies for example by Xing et al. [14] and Nejad et al. [15].

(a) 5MW wind turbine model in
SIMO-RIFLEX-AeroDyn
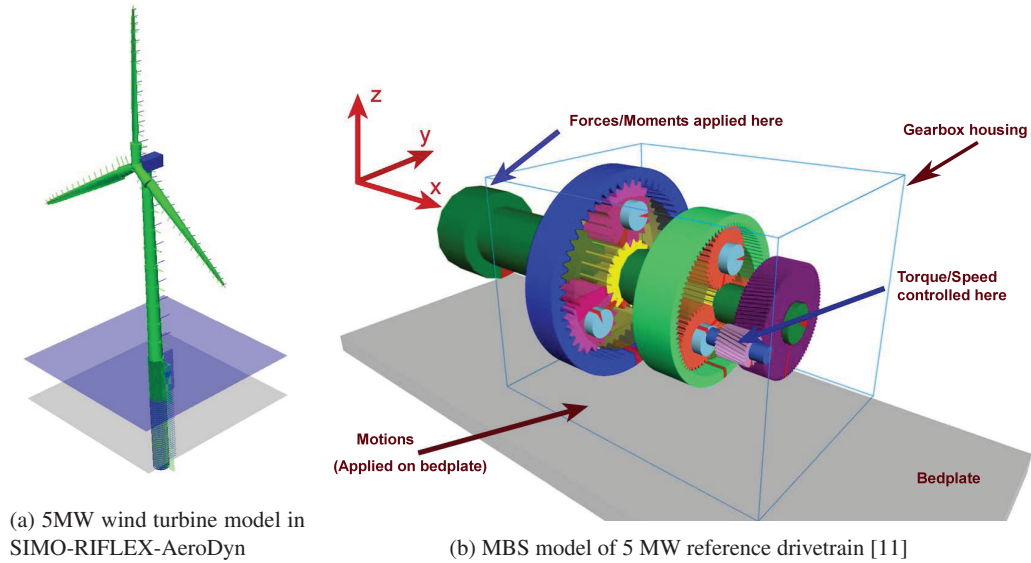
(b) MBS model of 5 MW reference drivetrain [11]

Fig. 2: Decoupled modelling

In the global analysis, the structure (monopile, tower, and blades) was modelled with beam elements, with additional point masses and inertias to represent the hub and nacelle. The soil effects were modelled through nonlinear springs distributed along the monopile, where the spring stiffness was given by [12]. Aerodynamic loads were computed according to the generalized dynamic wake (GDW) theory for $U_w \geq 8$ m/s and the blade element momentum (BEM) theory for $U_w < 8$ m/s. The wind turbine control system was included in the simulations, using the look-up table for generator torque and PI blade pitch controller from the NREL 5 MW definition [8]. Hydrodynamic loads on the monopile were calculated using Morison's equation (with $C_a = 1.0$ and $C_d = 0.9$) based on linear wave kinematics integrated up to the instantaneous undisturbed wave elevation.

The global analysis (Fig. 2a) was conducted for 24 load cases described in the last section. In order to reduce the statistical uncertainty, 6 simulations were carried out for each environmental condition. The force, moments and motions were then applied on a detailed drivetrain model. The multibody model of the drivetrain (MBS) was made in the SIMPACK [16] software and simulations were carried out for the selected cases shown in the Table 2.

Figure 2b shows the MBS model of the drivetrain. More details about this model and specification of gears and bearings can be found in Nejad et al. [11].

3.3. Gears & Bearings

Roller or anti friction bearings are commonly used in the wind turbine drivetrains. Spherical roller bearings, cylindrical roller bearings and taper roller bearings are the most common used. The roller bearings' fatigue life is a function of applied loads and is expressed by [3]:

$$L = \left(\frac{C}{P}\right)^a \tag{2}$$

in which L is the bearing basic life defined as the number of cycles that 90% of an identical group of bearings achieve, under a certain test conditions, before the fatigue damage appears. C is the basic load rating and is constant for a given bearing. The parameter $a = 3$ for ball bearing and $a = \frac{10}{3}$ for roller bearings. P is the dynamic equivalent load calculated from [17]:
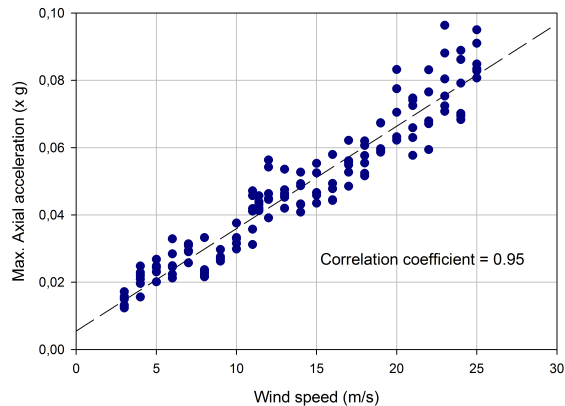
$$P = XF_r + YF_a \tag{3}$$

Fig. 3: Max. axial acceleration vs. wind speed.

where F_a and F_r are the axial and radial loads on the bearing respectively and X and Y are constant factors obtained from the bearing manufacturer.

The gears are designed based on the tooth root bending fatigue and surface pitting [18,19]. Both root bending stress and surface contact stress are related to the gear transmitted force or mesh force applied on the gear tooth which is a function of transmitted torque and gear internal dynamics [20,21].

In this study the correlation between the maximum equivalent load for bearings and mesh force for gears versus the maximum axial acceleration is investigated. These are good indicators of the fatigue life of gears and bearings in the drivetrain. The gears and bearings are chosen based on their fatigue ranking [22] as shown in Nejad et al. [11].

4. Results & Discussions

From the global response, torque, rotor bending moment and axial force are the design drivers for the drivetrain components. Figure 3 shows that the maximum of the axial acceleration at tower-top increases as wind increases. The maximum axial acceleration observed for this case study monopile offshore wind turbine is about $0.1g$, which occurs at high wind speeds near cut-out. The axial acceleration is shown as a factor of g with the $g = 9.81 m/s^2$. The coordinate system is shown in Figure 2b.

The frequency spectrum of the axial acceleration a_x for different environmental conditions - see Figure 4 - presents that a_x is not only influenced by the wind, but also by the wave and the first tower bending moment frequency - note that the vertical axis is in logarithmic scale.

For the low wind conditions, up to EC8, no wave frequency is observed in the a_x spectrum. The wave frequency appears for EC9 to EC14. This figure also indicates that the tower bending moment- which is excited by wind and wave loads and is seen by the nacelle as an external motion- is most dominant near cut-out wind speed, while rotational frequencies (e.g. $3P$) are dominant in other environmental conditions.

It is important to evaluate the load effects from the global analysis point of view before investigating the results from the local gearbox MBS simulations. The axial force on the tower top is apparently influenced by the axial acceleration. This force is particularly important for the main bearing design. Figure 5 shows the maximum of axial force F_x versus the maximum of the axial acceleration a_x. These are the peak values of each 10 min. simulation which have not necessarily occurred at the same time. Different trends are found for below -and above- rated wind speeds. This highlights the fact that the axial force is mainly dominated by the thrust force than the inertia force due to axial acceleration only. This fact can be seen in Figure 6 where the wind speed itself and the thrust force are shown as a function of the mean wind speed.

The bending moment at the tower top is another important load in designing the main shaft and the main bearings. It is interesting to observe that this moment, as shown in Figure 7, increases with the wind speed, very similar to
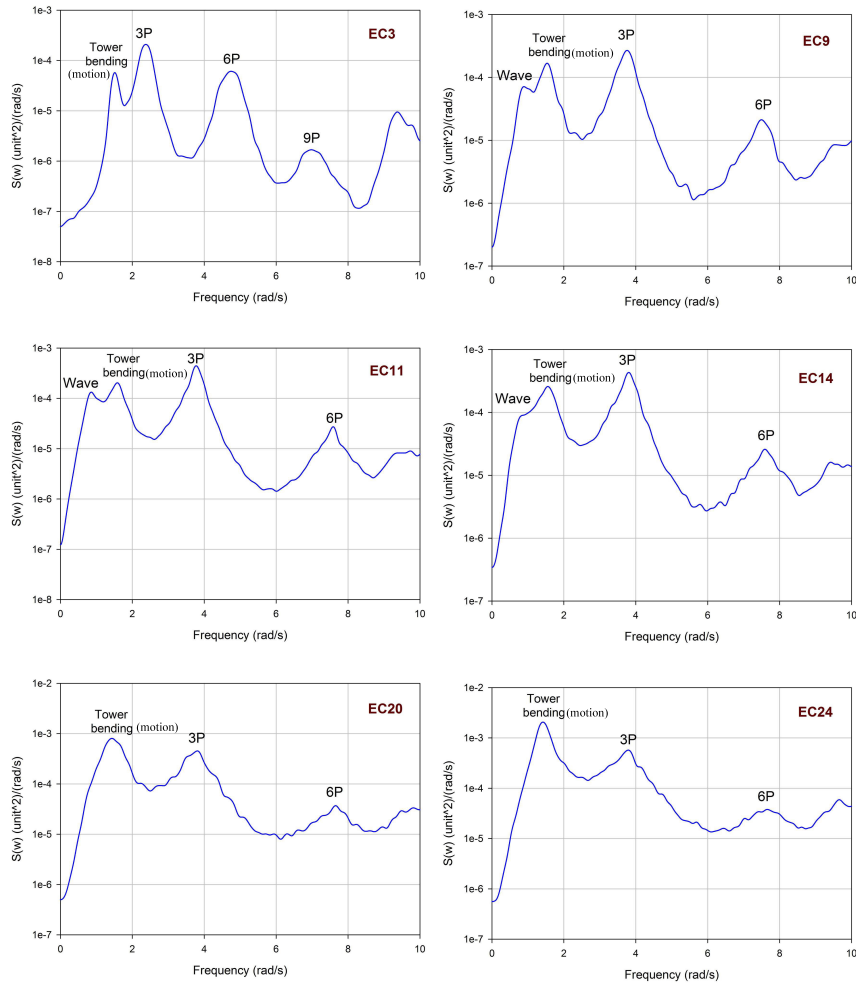
Fig. 4: Spectrum of axial acceleration (a_x) in different environmental conditions.

the axial acceleration. It also increases with the axial acceleration. However, this trend does not imply that the bending moment and the axial acceleration are correlated because the bending moment is not a direct function of the axial acceleration. While the axial force depends on thrust and inertia forces due to acceleration, the shaft bending moment depends on the moment due to uneven wind load on the rotor as well as uneven inertia forces caused by rotor acceleration.

Additionally, the load and fatigue responses in the monopile and tower can also be examined for correlation with the maximum acceleration or with the thrust force. Fig. 8 shows the normalized maximum bending moment, standard deviation of the bending moment, and fatigue damage as a function of the wind speed for several selected locations along the tower. The fatigue damage due to axial stress (at a point on the cross-section which is aligned with the wind and waves) was calculated using rainflow counting of the cycles and damage summation by Palmgren-Miner's rule. Bilinear SN curves for girth welds were used, following the DNV standard [23]. The probability of occurrence of the different environmental conditions is not accounted for.

As shown, the maximum bending moment generally follows the thrust force for lower sections of the monopile and tower, but increases more linearly with wind speed for points near the top of the tower. The fatigue damage is
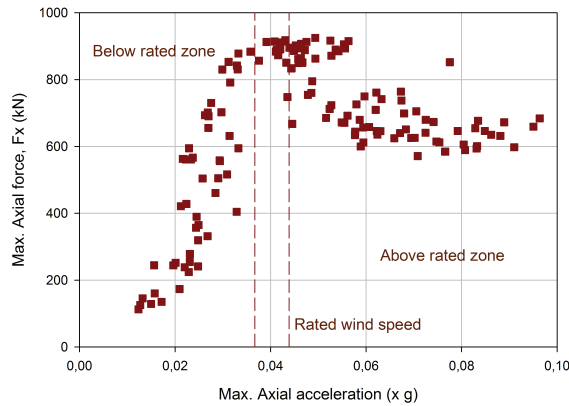
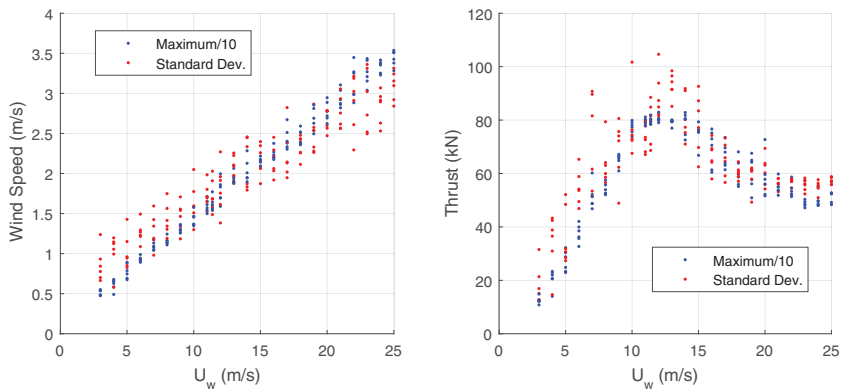Fig. 5: Max. axial force on tower-top vs. max. of axial acceleration.

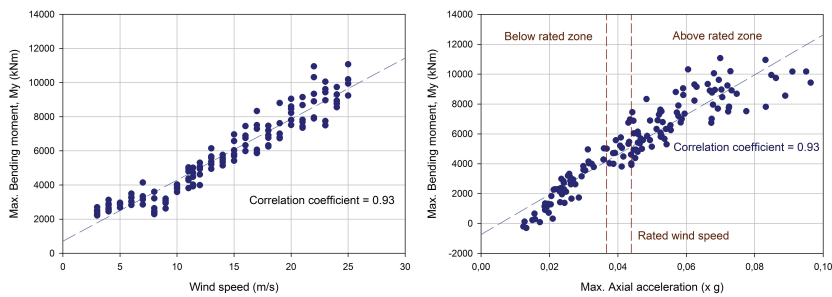Fig. 6: Max. and standard deviation of wind speed and thrust force vs. wind speed.

Fig. 7: Max. bending moment versus wind speed and max. axial acceleration.

greatest at the highest wind speeds for all cases, but the fatigue damage at the top of the tower is least affected by the rated wind speed.

The local drivetrain MBS simulation results for the selected load cases shown in table 2 were used for evaluating the components - see Figure 1 for the component names. The maximum equivalent load (equation 3) for the main
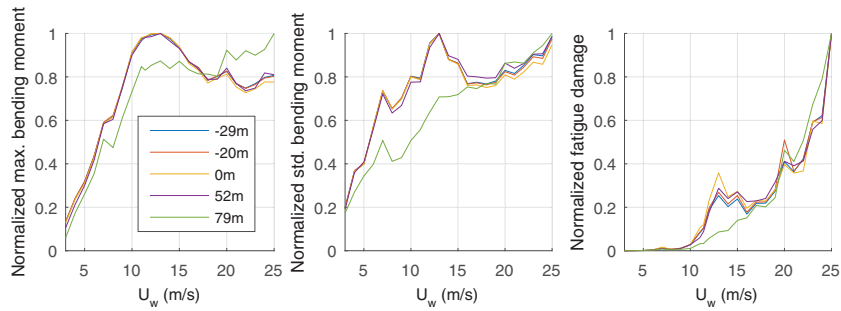
Fig. 8: Fore-aft bending moments and fatigue damage at selected points along the monopile and tower.
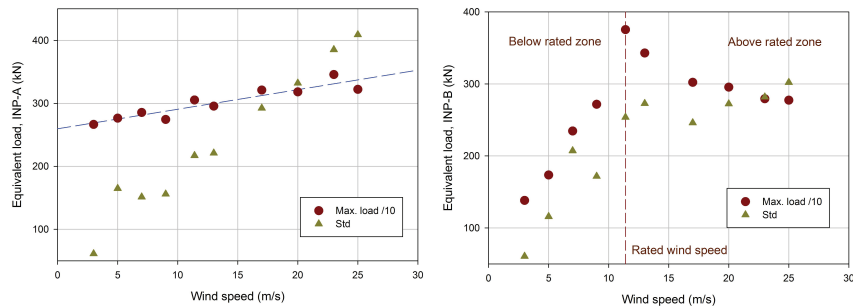

Fig. 9: Max. equivalent load of the main bearings (INP-A & INP-B) vs. wind speed.

bearings (INP-A and INP-B) versus the wind speed are shown in Figure 9. While INP-A appears to follow the wind, the INP-B load follows the axial force trend. This is due to the fact that the INP-B is the bearing which carries the axial force. The INP-A bearing is the one that carries the radial load induced by the bending moment on the shaft, thus its trend is similar to the bending moment and increases with the wind speed as well as axial acceleration since axial acceleration increases with the wind speed.

From the bearings inside the gearbox, one bearing (HS-C) in the high speed stage is selected as the bearings in high speed stage have the highest probability of fatigue failure. The maximum of the equivalent load for HS-C versus the wind speed is shown in Figure 10. A different trend below and above rated is observed, which highlights that the bearing load, and eventually its fatigue life, is not correlated with the axial acceleration and follows the torque or power curve.

For gears, the mesh force for the first stage sun gear is plotted versus the wind speed, see Figure 10. The gear mesh force, as it was shown by Nejad et al. [20], is primarily function of the input torque, thus the correlation with axial acceleration is not expected.

5. Concluding Remarks

In this paper the effect of the maximum axial acceleration at tower-top on the drivetrain was evaluated. A 5 MW monopile offshore wind turbine was selected and simulations for a range of environmental conditions from cut-in to cut-out considering both wave and wind were carried out. The forces, moments and motions from the global simulations were then applied on a detailed MBS model of the drivetrain.

The results showed that the maximum tower-top acceleration is about $0.1g$ for this monopile case study. The axial acceleration increases as the wind speed increases. It was also noticed that the acceleration is influenced by the rotational frequency, wave and tower bending frequencies with different intensity in different environmental conditions.
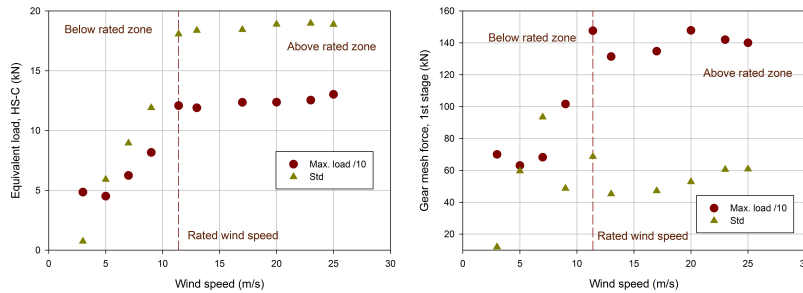
Fig. 10: Max. equivalent load of the high speed stage bearing (HS-C) and 1st stage gear mesh force vs. wind speed.

The effect of waves on tower top acceleration is observed below and near-rated wind speed, while tower motion has the highest impact at high wind speed.

No correlation was found between the maximum axial force on the tower-top and the maximum axial acceleration. The axial force follows the thrust force mainly. In a 4-point support configuration, the axial force on the main shaft is the design driver for the second main bearing. For 3-point support designs, a single main bearing carries both radial and axial forces.

The tower-top bending moment was found to increase as the wind increases. Knowing that the bending moment is a design driver for the main shaft and the main bearing, it therefore can be indicated that the size of the main shaft and the main bearing is directly correlated with the operational window.

The load effect of the components, gears and bearings, inside the gearbox were found to be not correlated with the axial acceleration. They mainly follow the torque and are influenced by the power control system.

The results of this work indicate that the maximum axial acceleration in the monopile offshore wind turbine is primarily a function of the tower motion, which is not a design driver for the drivetrain, and drivetrain design drivers - such as axial force, bending moment and the torque - are not necessarily correlated with the tower motion. Therefore the axial acceleration limit does not appear to be a rational criterion for the drivetrain design of monopile offshore wind turbines. However, this conclusion can not be generalized for floating wind turbines and thus the future work is devoted to investigate the effect of tower-top axial acceleration on the drivetrain in floating wind turbines.

Acknowledgements

References

[1] European Wind Energy Association. The European offshore wind industry - key trends and statistics 1st half 2015. Technical report, European Wind Energy Association (EWEA), 2015.
[2] IEC 61400-3. Wind turbines, Part 3: Design requirements for offshore wind turbines, 2009.
[3] IEC 61400-4. Wind turbines, Part 4: Standard for design and specification of gearboxes, 2012.
[4] Andersen L.V., Vahdatirad M.J., Sichani M.T., and Srensen J.D. Natural frequencies of wind turbines on monopile foundations in clayey soils-A probabilistic approach. *Computers and Geotechnics*, 43:1 – 11, 2012.
[5] Bachynski EE. and Moan T. Design considerations for tension leg platform wind turbines. *Marine Structures*, 29(1):89–114, 2012.
[6] Xing Y., Karimirad M., and Moan T. Modelling and analysis of floating spar-type wind turbine drivetrain. *Wind Energy*, 17:565–587, 2014.
[7] Nejad A.R., Bachynski EE., Kvittem M.I., Luan C., Gao Z., and Moan T. Stochastic Dynamic Load Effect and Fatigue Damage Analysis of Drivetrains in Land-based and TLP, Spar and Semi-Submersible Floating Wind Turbines. *Marine Structures*, 42:137–153, 2015.

[8] Jonkman J., Butterfield S., Musial W., and Scott G. Definition of a 5-MW reference wind turbine for offshore system development. Technical Report NREL/TP-500-38060, US National Renewable Energy Laboratory (NREL), 2009.

[9] Ormberg H. and Bachynski EE. Global analysis of floating wind turbines: Code development, model sensitivity and benchmark study. In *22nd International Ocean and Polar Engineering Conference*, volume 1, pages 366–373, 2012.

[10] Li L., Gao Z., and Moan T. Joint long-term environmental conditions at five European offshore sites for design of combined wind and wave energy devices. *Journal of Offshore Mechanics and Arctic Engineering*, 137(3):031901, 2015.

[11] Nejad A.R., Guo Y., Gao Z., and Moan T. Development of a 5 MW reference gearbox for offshore wind turbines. *Wind Energy*, DOI:10.1002/we.1884, 2015.

[12] J. Jonkman, S. Butterfield, P. Passon, T. J Larsen, T. Camp, J. Nichols, J. Azcona, and A. Martinez. Offshore code comparison collaboration within IEA Wind Annex XXIII: Phase II results regarding monopile foundation modeling. In *IEA European Offshore Wind Conference*, Berlin, Germany, December 2007.

[13] Nejad A.R. *Dynamic analysis and design of gearboxes in offshore wind turbines in a structural reliability perspective*. Norwegian University of Science and Technology (NTNU), Department of Marine Technology, Ph.D. thesis, No. 191, 2015.

[14] Xing Y. and Moan T. Multibody modelling and analysis of a planet carrier in a wind turbine gearbox. *Wind Energy*, 16(7):1067–1089, 2013.

[15] Nejad A.R., Odgaard P.F., Gao Z., and Moan T. A prognostic method for fault detection in wind turbine drivetrains. *Engineering Failure Analysis*, 42:324 – 336, 2014.

[16] SIMPACK. Multi body system software. `www.simpack.com/`. [Online; accessed 24-Dec-2015].

[17] ISO 281. Rolling bearings - dynamic load ratings and rating life, 2007.

[18] ISO 6336-2. Calculation of load capacity of spur and helical gears, Part 2: Calculation of surface durability (pitting), 2006.

[19] ISO 6336-3. Calculation of load capacity of spur and helical gears, Part 3: Calculation of tooth bending strength, 2006.

[20] Nejad A.R., Gao Z., and Moan T. On long-term fatigue damage and reliability analysis of gears under wind loads in offshore wind turbine drivetrains. *International Journal of Fatigue*, 61:116–128, 2014.

[21] Nejad A.R., Gao Z., and Moan T. Long-term analysis of gear loads in fixed offshore wind turbines considering ultimate operational loadings. *Energy Procedia*, 35:187–197, 2013.

[22] Nejad A.R., Gao Z., and Moan T. Fatigue reliability-based inspection and maintenance planning of gearbox components in wind turbine drivetrains. *Energy Procedia*, 53:248–257, 2014.

[23] Det Norske Veritas. Fatigue design of offshore steel structures. Technical Report DNV-RP-C203, 2010.